AIMS Mathematics, 10(12): 29107–29131.
DOI: 10.3934/math.20251280
Received: 04 November 2025
Revised: 28 November 2025
Accepted: 03 December 2025
Published: 11 December 2025

https://www.aimspress.com/journal/Math

Research article

Model-independent multi-target tracking of networked marine surface vehicles with predefined-time convergence performance

Xionghua Liu[1,2], Yang Zhang[3], Kai-Lun Huang[2], Jing-Zhe Xu[1] and Chang-Duo Liang[3,*]

[1] School of Artificial Intelligence and Automation, Huazhong University of Science and Technology, Wuhan 430074, China

[2] School of Computer Science and Automation, Wuhan Technology and Business University, Wuhan 430065, China

[3] School of Electrical Engineering and Automation, Hubei Normal University, Huangshi 435002, China

* **Correspondence:** Email: cdliang@hbnu.edu.cn.

Abstract: This paper mainly focuses on the model-independent multi-target tracking problem of the networked marine surface vehicles (NMSVs) while requiring that the settling time is limited to a predefined one. For addressing such a complex problem, a hierarchical control framework is employed, consisting of a predefined-time distributed estimator (PDE) algorithm and a model-independent predefined-time local tracking (MPLT) algorithm. To be specific, the PDE algorithm aims to estimate the virtual leaders states in a distributed fashion within a predefined time, so that each vehicle obtains its corresponding leaders' information. Based on these estimations, the MPLT algorithm is designed to achieve predefined-time multi-target tracking of the NMSVs. By conducting a rigorous Lyapunov stability analysis, the sufficient conditions guaranteeing the predefined-time stability of the closed-loop system are derived. Subsequently, simulation studies are presented to demonstrate the feasibility and superiority of the proposed approach.

Keywords: distributed model-independent control; multi-target tracking; networked marine surface vehicles; predefined-time stability
Mathematics Subject Classification: 34D20, 93B52, 93C10, 93C85

1. Introduction

The growing global demand for ocean resource exploration has intensified research on advanced control strategies for marine surface vehicles, as increasingly complex maritime missions such as environmental monitoring [1], hydrogeological surveying [2], and search and rescue operations [3]

can no longer be accomplished by a single vehicle alone. Consequently, motivated by the principles of multi-agent systems, including distributed tracking [4, 5], formation tracking [6, 7], and flocking [8], increasing attention has been devoted to the automation and distributed control of networked marine surface vehicles (NMSVs). In recent work, the robustness and resilience of complex networks under uncertainty and disturbance have been explored, providing valuable insights for the cooperative control of networked marine surface vehicles [9]. Additionally, research on conflict resolution for multiple unmanned aerial vehicles (UAVs) has highlighted the importance of decentralized decision-making and cooperative control in multi-agent systems [10]. These findings are particularly relevant as NMSVs consist of multiple vehicles interconnected through a communication network, embodying the principles of multi-agent systems theory. The cooperative framework of NMSVs provides flexibility to adapt to time-varying and uncertain ocean conditions, ensuring high reliability, improved energy efficiency, broader operational coverage, and superior robustness compared to single-vehicle systems. Accordingly, the study of distributed control strategies for NMSVs carries not only theoretical significance but also considerable practical value for enhancing maritime safety, operational efficiency, and mission reliability in realistic marine applications.

In the context of maritime cooperative missions, the multi-target tracking problem of NMSVs refers to the scenario in which multiple vehicles are required to simultaneously converge toward distinct equilibrium states associated with their respective targets. Despite its importance, most existing investigations on the tracking problem have concentrated on the distributed tracking of a single target [11, 12]. The findings presented in these studies, however, are not directly transferable to situations where a networked system must accomplish several independent objectives at the same time. This limitation has encouraged a number of recent efforts addressing topics such as multi-consensus [13, 14], multi-tracking [15, 16], and multi-formation [17, 18]. Nevertheless, from an engineering perspective, describing such agents merely through single- or double-integrator models is an oversimplification that neglects the inherent physical dynamics of marine vehicles. This simplification becomes particularly inadequate for NMSVs, whose behavior is more accurately captured by Euler-Lagrange formulations. Therefore, from a system-theoretic viewpoint, it is of greater significance to investigate the cooperative control of NMSVs, which serve as representative real-world implementations [19].

The surge-sway-yaw dynamics of NMSVs are inherently sensitive to variations in operating conditions, including forward velocity, attitude changes, and sea-state fluctuations. Such sensitivity makes the system particularly vulnerable to model uncertainties and environmental disturbances, which often deteriorate the overall control performance. To counteract these challenges, a variety of control methodologies have been introduced in recent years, including observer-based control [20], adaptive control [21], and neural network-based control [22]. Nevertheless, accurately identifying the underlying hydrodynamic parameters, including the mass, Coriolis, and damping matrices, remains a labor-intensive and unreliable process, often leading to inconsistencies between offline model characterization and real-time system behavior. Many of the aforementioned methods still depend on partial model knowledge within the controller design, thereby constraining their effectiveness in scenarios where such information cannot be accurately obtained. This limitation has encouraged the development of an alternative paradigm in the control field, commonly referred to as model-independent control [23, 24]. In this work, a model-independent framework is adopted, where all unknown dynamic terms and external disturbances are considered an equivalent disturbance

channel and compensated in real time through a super-twisting observer, ensuring strong robustness against modeling errors and variations in sea conditions.

In marine coordination control, optimizing convergence speed has long been considered a critical issue, especially under practical operational constraints such as oceanic deployment schedules, tide and weather windows, and limited communication duty cycles. A considerable body of research has been devoted to achieving various stability objectives of the systems, including asymptotic stability [25], finite-time stability [26], and fixed-time stability [27]. Nevertheless, the settling times associated with these frameworks remain restricted by inherent limitations. Specifically, the convergence duration for asymptotic stability theoretically approaches infinity, the finite-time settling time depends on the initial state conditions, and the fixed-time convergence bound is implicitly coupled with the control and system parameters, making its determination complex. To address these drawbacks, the notion of predefined-time stability was proposed [28, 29], in which the upper bound of convergence time can be explicitly prescribed through controller parameters. Despite its advantages, existing predefined-time control methods are predominantly established for second-order system models, with relatively few studies extending this framework to the coordination of NMSVs. Therefore, developing a predefined-time control scheme tailored to the multi-target tracking of NMSVs holds both theoretical significance and practical relevance for high-performance marine cooperative missions.

Motivated by the above discussions, this work develops a hierarchical model-independent predefined-time control framework for multi-target tracking of NMSVs over directed multi-leader graphs. The coordination layer employs a predefined-time distributed estimator to reconstruct each leader's motion states using integral sliding-mode principles and pinning communication, while the execution layer implements a predefined-time local tracking controller that ensures accurate earth-fixed convergence through a smooth sliding manifold and real-time disturbance compensation via a super-twisting observer. The major contributions of this work are summarized as follows.

- A hierarchical predefined-time control framework is proposed for multi-target tracking of NMSVs. The coordination layer employs a distributed predefined-time estimator (PDE) to reconstruct each leaderis motion states via integral sliding-mode principles and pinning communication, while the local layer ensures earth-fixed convergence through a predefined-time tracking law.
- Unlike single-target coordination approaches [11, 12] or existing single-vehicle, single-target tracking methods [30, 31], this study addresses a multi-target tracking problem where each vehicle converges to its designated equilibrium under a directed multi-leader topology, enabling simultaneous coordination toward multiple distinct objectives.
- Compared with model-based control approaches that explicitly depend on system parameters (see [20–22]), the proposed method eliminates the need for prior model identification. A model-independent predefined-time local tracking (MPLT) algorithm is developed, in which all unknown dynamics and external disturbances are unified into an equivalent disturbance channel and compensated in real time through a super-twisting observer, without requiring any hydrodynamic matrices in the controller design.

Notations: $\mathbb{R}$ and $\mathbb{R}^n$ denote the sets of real numbers and n-dimensional real vectors, respectively. "$\otimes$" and "$\circ$" represent the Kronecker and Hadamard product operations. For given

$$m = [m_1, m_2, \ldots, m_n] \in \mathbb{R}^n \quad \text{and} \quad \alpha \in \mathbb{R},$$

$$\mathrm{sig}^{\alpha}(m) = [|m_1|^{\alpha}\mathrm{sgn}(m_1), \ldots, |m_n|^{\alpha}\mathrm{sgn}(m_n)]^T, \quad \langle m \rangle^{\alpha} = [m_1^{\alpha}, \ldots, m_n^{\alpha}]^T.$$

For given $m, n \in \mathbb{R}^n$,

$$\mathrm{col}(m, n) = [m^T, n^T]^T$$

means the column operation.

2. Preliminaries

2.1. Graph theory

A directed graph

$$\mathcal{G} = \{\mathcal{V}, \mathcal{E}, \mathcal{A}\}$$

is utilized to characterize the communication topology among the N networked NMSVs. Specifically,

$$\mathcal{V} = \{1, 2, \ldots, N\} \in \mathbb{R}^N$$

denotes the set of vertices,

$$\mathcal{E} = \{e_{ij} = (i, j) \,|\, i, j \in \mathcal{V}\} \subseteq \mathcal{V} \times \mathcal{V}$$

represents the set of directed communication edges, and

$$\mathcal{A} = [a_{ij}] \in \mathbb{R}^{N \times N}$$

corresponds to the associated adjacency matrix. In this framework, an edge $e_{ij} \in \mathcal{E}$ indicates that agent i can directly receive information from agent j. Conversely, the existence of $e_{ji} \in \mathcal{E}$ implies the reverse direction of information transmission. Accordingly, if $e_{ij} \in \mathcal{E}$, one has $a_{ij} \neq 0$; otherwise, $a_{ij} = 0$. Moreover, $a_{ij} > 0$ signifies a cooperative interaction between agents i and j, while $a_{ij} < 0$ denotes a competitive relation. It is further assumed that $\mathcal{G}$ contains no self-loops, i.e., $a_{kk} = 0$ for all $k \in \mathcal{V}$. The Laplacian matrix associated with $\mathcal{G}$ is denoted as

$$\mathcal{L} = [l_{ij}] \in \mathbb{R}^{N \times N},$$

where $l_{ij} = -a_{ij}$ for $i \neq j$ and

$$l_{ii} = \sum_{k=1}^{N} a_{ik}$$

for $i \in \mathcal{V}$.

Furthermore, the multi-target tracking scenario is organized under the guidance of M_l virtual leaders. Accordingly, the overall communication graph $\mathcal{G}$ can be partitioned into M_l subgroups, each represented by a subgraph

$$\mathcal{G}_l = \{\mathcal{V}_l, \mathcal{E}_l, \mathcal{A}_l\},$$

where $l \in \{1, 2, \ldots, M_l\}$ corresponds to the lth leader. The associated Laplacian matrix $\mathcal{L}$ is then expressed in a block-matrix form

$$\mathcal{L} = [\mathcal{L}_{mn}], \;\; m, n \in \{1, 2, \ldots, M_l\},$$

in which $\mathcal{L}_{mn}$ characterizes the interconnections between subgroups m and n for $m \neq n$ and reduces to the Laplacian matrix of subgraph $\mathcal{G}_m$ when $m = n$. It is further assumed that each vehicle belongs exclusively to one subgroup. In addition, a diagonal pinning matrix

$$\mathcal{B} = \text{diag}\{b_1, b_2, \ldots, b_N\} \in \mathbb{R}^{N\times N}$$

is introduced to describe the communication links between the vehicles and their respective virtual leaders. Specifically, $b_k > 0$ indicates that vehicle k can directly receive information from its corresponding leader, whereas $b_k = 0$ implies no direct connection.

Finally, two standard assumptions concerning the multi-leader network topology are introduced as follows.

Assumption 1. *Each subgraph combined with the corresponding leader has a spanning tree with the leader being the rooted node.*

Assumption 2. *The total cooperation and competition communication weight between any two subgroups are balanced, i.e., $\mathcal{L}_{mn}\mathbf{1} = \mathbf{0}$ for any $m \neq n \in \{1, 2, \ldots, M_l\}$.*

2.2. Predefined-time sliding mode surface

Before introducing the predefined-time terminal sliding mode surface, the definition of the time regulation function is presented here.

Definition 1. *(Time regulate function) For a time-based variable $\xi(t) \in \mathbb{R}$, a constructed function $\hbar(\xi(t)) \in \mathbb{R}$, of which the value range is $[-1, 1]$, is called a time regulator function if it satisfies the following conditions:*

- *$\hbar(\xi(t))$ is a continuous function that is at least twice differentiable for all $t \in [0, +\infty)$.*
- *For any $t \in [0, +\infty)$, $\hbar(\xi(t)) = 0$ holds if and only if $\xi(t) = 0$.*
- *The time derivative $\dot{\hbar}(\xi(t))$ remains nonzero for all $t \in [0, +\infty)$.*

Remark 1. *When employing the time regulate function in the case of vector form, i.e.,*

$$\xi(t) = [\xi_1(t), \xi_2(t), \ldots, \xi_n(t)] \in \mathbb{R}^n,$$

it is defined that

$$\hbar(\xi(t)) = [\hbar_1(\xi(t), \hbar_2(\xi(t), \ldots, \hbar_n(\xi(t)]^T, \quad \frac{\mathrm{d}\hbar(\xi(t))}{\mathrm{d}\xi(t)} = [\frac{\mathrm{d}\hbar(\xi_1(t))}{\mathrm{d}\xi_1(t)}, \frac{\mathrm{d}\hbar(\xi_2(t))}{\mathrm{d}\xi_2(t)}, \ldots, \frac{\mathrm{d}\hbar(\xi_n(t))}{\mathrm{d}\xi_n(t)}]^T.$$

Further, two kinds of predefined-time sliding mode surfaces that will be in the subsequent controller design are introduced here, which are detailedly presented as follows:

- *Nonsingular predefined-time sliding mode surface [32]*:

$$\sigma = \hbar(\xi) + \left[\mathcal{T}_s\left(1 - \frac{\gamma_1}{\gamma_2}\right)\right]^{\frac{\gamma_2}{\gamma_1}} \text{sig}(\dot{\hbar}(\xi))^{\frac{\gamma_2}{\gamma_1}}, \tag{2.1}$$

where $\xi \in \mathbb{R}$ is the system state, and γ_1, γ_2 are positive odd integers satisfying $\gamma_1 < \gamma_2 < 2\gamma_1$.

- *Integral predefined-time sliding mode surface [33]*:

$$\sigma = \xi + \frac{1}{\mathcal{T}_s(1-\gamma)} \int_0^t \left(\frac{d\hbar(\xi(\tau))}{dx(\tau)} \right)^{-1} \text{sig}(\hbar(\xi(\tau)))^{\gamma} d\tau, \tag{2.2}$$

  where $0 < \gamma < 1$.

In the above sliding mode surfaces, $\mathcal{T}_s$ is the predefined-time parameter, namely, ξ will be forced to zero within $t \leq \mathcal{T}_c$ after $\sigma = 0$ is reached.

2.3. Useful lemmas

Some useful lemmas that would be employed in the stability analysis part are organized in this subsection.

Lemma 1. *[32] Consider the differential system*

$$\dot{\xi} = f(t, \xi), \;\; \xi(0) = \xi_0,$$

where $\xi \in \mathbb{R}^n$ is the system state. If the constructed Lyapunov function

$$V(\xi) : \mathbb{R}^n \mapsto \mathbb{R}$$

satisfies that

$$\dot{V}(\xi) \leq -\frac{\vartheta}{\mathcal{T}} \Big[\alpha V^{\rho}(\xi) + \beta V^{\ell}(\xi) \Big]^k, \;\; \forall \xi \in R^n / \{0\}, \tag{2.3}$$

where $\mathcal{T}_c > 0$ is the predefined-time parameter, $\rho, \ell, k, \alpha, \beta > 0$ with $k\rho < 1$, $k\ell > 1$,

$$\vartheta = \frac{\Gamma\left(m_{\rho}\right) \Gamma\left(m_{\ell}\right)}{\alpha^k \Gamma(k)(\ell - \rho)} \left(\frac{\alpha}{\beta} \right)^{m_{\rho}},$$

in which

$$m_{\rho} = (1 - k\rho)/(\ell - \rho), \;\; m_{\iota} = (k\ell - 1)/(\ell - \rho),$$

and $\Gamma(\cdot)$ is the Gamma function, then the considered system is predefined-time stable with settling time being $t \leq \mathcal{T}_c$.

Lemma 2. *[34] Consider the differential system in Lemma 1. If the constructed positive-definite Lyapunov function*

$$V(\xi) : \mathbb{R}^n \mapsto \mathbb{R}$$

satisfies that

$$\dot{V}(\xi) \leq -k_1 V(\xi) - \frac{2}{k_2} \frac{\dot{\wp}(t, \mathcal{T}_c)}{\wp(t, \mathcal{T}_c)} V(\xi) \tag{2.4}$$

with $\mathcal{T}_c, k_1, k_2 > 0$, and

$$\wp(t, \mathcal{T}_c) = \begin{cases} \frac{\mathcal{T}_c{}^h}{(\mathcal{T}_c + t_0 - t)^h}, & t_0 \leq t < \mathcal{T}_c + t_0, \\ 1, & t \geq \mathcal{T}_c + t_0, \end{cases} \tag{2.5}$$

$$\dot{\wp}(t,\mathcal{T}_c)=\begin{cases}\frac{h}{\mathcal{T}_c}\wp^{\left(1+\frac{1}{h}\right)}, & t_0\le t<\mathcal{T}+t_0,\\ 0, & t\ge\mathcal{T}_c+t_0,\end{cases}\tag{2.6}$$

where $h>2$, then the system attains predefined-time stability; moreover, the settling time does not exceed $\mathcal{T}_c$, i.e., $t\le\mathcal{T}_c$.

Lemma 3. *[35] Consider the super-twisting dynamics expressed as*

$$\dot{x}=-\kappa_1\mathrm{sig}(x)^{1/2}+y,\ \ \dot{y}=-\kappa_2\mathrm{sgn}(x)+f(t),$$

with initial values $x(0)=x_0$ and $y(0)=y_0$, where $x,y\in\mathbb{R}^n$ denote the system states and $f(t)$ is a time-varying vector function. Assume the existence of a constant $\zeta_f>0$ such that

$$\|f(t)\|\le\zeta_f$$

holds for all t. When the control parameters satisfy

$$\kappa_1\ge1.5\sqrt{\zeta_f}$$

and $\kappa_2\ge1.1\zeta_f$, the origin

$$(x,y)=(0,0)$$

is finite-time stable. In other words, the trajectories $x(t)$ and $y(t)$ reach zero within a finite time, and the corresponding settling time satisfies

$$t\le\mathcal{T}(x_0,y_0).$$

3. Model and problem formulation

3.1. NMSVs model description

Prior to establishing the mathematical model, the earth-fixed and body-fixed coordinate frames are defined as illustrated in Figure 1.

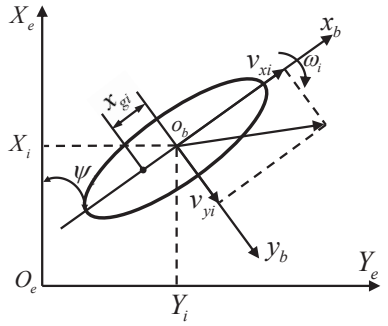

Figure 1. The body-fixed coordinates $x_bo_by_b$ and the earth-fixed coordinates $X_eO_eY_e$ of NMSVs.

Assuming that each vehicle possesses port-starboard symmetry, the dynamic model of the ith vehicle can be formulated as follows:

$$\begin{cases}\dot{\eta}_i=R_i(\psi_i)\,v_i,\\ M_i\dot{v}_i+C_i(v_i)\,v_i+D_i(v_i)\,v_i=\tau_i+\tau_{d,i},\end{cases}\tag{3.1}$$

where

$$\eta_i = [X_i, Y_i, \psi_i]^T$$

and

$$v_i = [v_{xi}, v_{yi}, \omega_i]^T \in \mathbb{R}^3$$

denote the position-attitude vector in the earth-fixed frame $X_eO_eY_e$ and the velocity-angular-rate vector in the body-fixed frame $x_bO_by_b$, respectively. The control input $\tau_i \in \mathbb{R}^3$ represents the physical control vector, and

$$\tau_{d,i} = M_i R_i^T(\psi_i) d_i(t) \in \mathbb{R}^3$$

accounts for the external disturbance effects, where $d_i(t)$ denotes the disturbance vector. $\tau_{d,i}$ and $M_i R_i^T(\psi_i) d_i(t)$ represent mathematically equivalent expressions of the same underlying disturbance. The rotation matrix $R_i(\psi_i)$ and the dynamic matrices M_i, $C_i(v_i)$, and $D_i(v_i) \in \mathbb{R}^{3\times3}$ are defined in [36, 37] for detailed formulation. Let

$$\varpi_i \triangleq \dot{\eta}_i = [V_{Xi}, V_{Yi}, \omega_i]^T$$

denote the velocity vector expressed in the earth-fixed frame. Accordingly, the physical plant model of the ith vehicle can be rewritten as

$$\bar{M}_i(\eta_i)\ddot{\eta}_i + \bar{C}_i(\eta_i, \dot{\eta}_i)\dot{\eta}_i + \bar{D}_i(\eta_i, \dot{\eta}_i)\dot{\eta}_i = R_i(\psi_i)\tau_i + \bar{M}_i(\eta_i) d_i(t), \tag{3.2}$$

where the newly obtained dynamical matrices are presented as

$$\begin{cases} \bar{M}_i(\eta_i) = R_i(\psi_i) M_i R_i^T(\psi_i), \\ \bar{C}_i(\eta_i, \dot{\eta}_i) = R_i(\psi_i)\left[C_i(v_i) - M_i R_i^T(\psi_i)\dot{R}_i(\psi_i)\right] R_i^T(\psi_i), \\ \bar{D}_i(\eta_i, \dot{\eta}_i) = R_i(\psi_i) D_i(v_i) R_i^T(\psi_i). \end{cases} \tag{3.3}$$

Here, the property that

$$R_i^T(\eta_i) R_i(\eta_i) = I$$

has been employed in the above evolution.

On the other hand, the trajectories of the M_l virtual leaders in the earth-fixed frame are governed by

$$\dot{\eta}_{0,l} = \varpi_{0,l}, \quad \dot{\varpi}_{0,l} = \mu_{0,l}, \quad l \in \{1, 2, \ldots, M_l\},$$

where $\eta_{0,l}$, $\varpi_{0,l}$, and $\mu_{0,l} \in \mathbb{R}^3$ represent the position-attitude, velocity-angular-rate, and acceleration vectors of the lth virtual leader in the earth-fixed coordinates, respectively.

Assumption 3. *The states $\eta_{0,l}$, $\varpi_{0,l}$, and $\mu_{0,l}$ of virtual leader are all bounded.*

3.2. Problem formulation

The main objective is to design a proper cooperative algorithm without the model information in a distributed way such that the NMSVs can realize the multi-target tracking within a predefined time. The specific mathematical definition is given below.

Definition 2. *The considered model-independent predefined-time multi-target tracking problem is addressed if*

$$\begin{cases} \lim\limits_{t\to\mathcal{T}_f} \left\|e_{\eta i,l}\right\| = 0, \\ \lim\limits_{t\to\mathcal{T}_f} \left\|e_{\varpi i,l}\right\| = 0, \end{cases} \forall i \in V_l, l \in \{1,2,\ldots,M_l\}, \tag{3.4}$$

and

$$\left\|e_{\eta i,l}\right\| = 0, \ \ \left\|e_{\varpi i,l}\right\| = 0$$

hold when $t \geq \mathcal{T}_f$, where

$$e_{\eta i,l} = \eta_i - \eta_{0,l}, \ \ e_{\varpi i,l} = \varpi_i - \varpi_{0,l}$$

are the tracking errors in the earth-fixed coordinates. $\mathcal{T}_f$ is the settling time that can be arbitrarily in the permitted time adjustment range $[\mathcal{T}_{per}, +\infty]$, where $\mathcal{T}_{per}$ is the permissible minimum value for adjusting the settling time, which would be determined by actual constraints, e.g., the observer process in our subsequent design work. Besides, it is noteworthy that no model information can be involved in the controller design.

4. Controller design

The main purpose of this section is to construct the distributed control algorithm for NMSVs in a model-free way with the consideration of the predefined-time multi-target tracking problem. To facilitate the solution of this challenging control problem, a hierarchical control architecture is introduced to alleviate the design complexity. In particular, a PDE is constructed to estimate the states of the virtual leaders, so that each vehicle can obtain, either directly or through its neighbors, the state information of its designated leader. Later, by using the obtained estimators as the reference trajectories, a MPLT algorithm will be proposed, actuating the NMSVs to reach the multi-target tracking. The two layers communicate by transferring the estimated states of the leaders from the PDE layer to the MPLT layer. The feedback control input generated by the MPLT layer drives the vehicles to track the leaders' trajectories, ensuring that multi-target convergence is achieved. This hierarchical structure simplifies the overall control design and allows for systematic separation of the estimation and tracking tasks, ensuring that each layer's role is well defined and independently optimized.

To begin, for building the PDE algorithm, estimators $\hat{\eta}_i, \hat{\varpi}_i, \hat{\mu}_i \in \mathbb{R}^3$ are introduced for vehicle i, aiming to track the states of the leaders, and the coordinated errors are defined as

$$\hat{E}_{\eta i} = \sum_{j\in\mathcal{N}_i} a_{ij}\left(\hat{\eta}_i - \hat{\eta}_j\right) + b_i\left(\hat{\eta}_i - \eta_{0,l}\right), \tag{4.1}$$

$$\hat{E}_{\varpi i} = \sum_{j\in\mathcal{N}_i} a_{ij}\left(\hat{\varpi}_i - \hat{\varpi}_j\right) + b_i\left(\hat{\varpi}_i - \varpi_{0,l}\right), \tag{4.2}$$

$$\hat{E}_{\mu i} = \sum_{j\in\mathcal{N}_i} a_{ij}\left(\hat{\mu}_i - \hat{\mu}_j\right) + b_i\left(\hat{\mu}_i - \hat{\mu}_{0,l}\right). \tag{4.3}$$

Further, according to Subsection 2.2, the following integral predefined-time sliding mode surfaces are constructed:

$$\hat{\sigma}_i = \hat{E}_{\eta i} + \frac{1}{\mathcal{T}_s(1-\gamma)} \int_0^t \left\langle \frac{\mathrm{d}\hbar\left(\hat{E}_{\eta i}(\sigma)\right)}{\mathrm{d}\hat{E}_{\eta i}(\sigma)} \right\rangle^{-1} \circ \mathrm{sig}\left(\hbar\left(\hat{E}_{\eta i}(\sigma)\right)\right)^{\gamma} \mathrm{d}\sigma, \tag{4.4}$$

$$\hat{n}_i = \hat{E}_{\varpi i} + \frac{1}{\mathcal{T}_s(1-\gamma)} \int_0^t \left\langle \frac{\mathrm{d}\hbar\left(\hat{E}_{\varpi i}(\sigma)\right)}{\mathrm{d}\hat{E}_{\varpi i}(\sigma)} \right\rangle^{-1} \circ \mathrm{sig}\left(\hbar\left(\hat{E}_{\varpi i}(\sigma)\right)\right)^{\gamma} \mathrm{d}\sigma, \tag{4.5}$$

$$\hat{m}_i = \hat{E}_{\mu i} + \frac{1}{\mathcal{T}_s(1-\gamma)} \int_0^t \left\langle \frac{\mathrm{d}\hbar\left(\hat{E}_{\mu i}(\sigma)\right)}{\mathrm{d}\hat{E}_{\mu i}(\sigma)} \right\rangle^{-1} \circ \mathrm{sig}\left(\hbar\left(\hat{E}_{\mu i}(\sigma)\right)\right)^{\gamma} \mathrm{d}\sigma, \tag{4.6}$$

where $\mathcal{T}_s > 0$ is the predefined-time parameters in the sliding mode vector design, $0 < \gamma < 1$, $\hat{E}_{\eta i}(0), \hat{E}_{\varpi i}(0), \hat{E}_{\mu i}(0)$ are the initial value vectors of $\hat{E}_{\eta i}, \hat{E}_{\varpi i}, \hat{E}_{\mu i}$.

Based on the above analysis, the PDE algorithm is developed as

$$\begin{cases} \dot{\hat{\eta}}_i = \hat{\pi}_{\eta i}, \ \ \dot{\hat{\varpi}}_i = \hat{\pi}_{\varpi i}, \ \ \dot{\hat{\mu}}_i = \hat{\pi}_{\mu i}, \\ \hat{\pi}_{\eta i} = \left[\sum\limits_{j\in\mathcal{N}_i} a_{ij} + b_i\right]^{-1} \left[\begin{array}{c} \sum\limits_{j\in\mathcal{N}_i} a_{ij}\hat{\pi}_{\eta j} - \rho(t)\hat{\sigma}_i + b_i\varpi_{0,l} \\ -\frac{1}{\mathcal{T}_s(1-\gamma)}\left\langle \frac{\mathrm{d}\hbar\left(\hat{E}_{\eta i}\right)}{\mathrm{d}\hat{E}_{\eta i}} \right\rangle^{-1} \circ \mathrm{sig}\left(\hbar\left(\hat{E}_{\eta i}\right)\right)^{\gamma} \end{array}\right], \\ \hat{\pi}_{\varpi i} = \left[\sum\limits_{j\in\mathcal{N}_i} a_{ij} + b_i\right]^{-1} \left[\begin{array}{c} \sum\limits_{j\in\mathcal{N}_i} a_{ij}\hat{\pi}_{\varpi j} - \rho(t)\hat{n}_i + b_i\mu_{0,l} \\ -\frac{1}{\mathcal{T}_s(1-\gamma)}\left\langle \frac{\mathrm{d}\hbar\left(\hat{E}_{\varpi i}\right)}{\mathrm{d}\hat{E}_{\varpi i}} \right\rangle^{-1} \circ \mathrm{sig}\left(\hbar\left(\hat{E}_{\varpi i}\right)\right)^{\gamma} \end{array}\right], \\ \hat{\pi}_{\mu i} = \left[\sum\limits_{j\in\mathcal{N}_i} a_{ij} + b_i\right]^{-1} \left[\begin{array}{c} \sum\limits_{j\in\mathcal{N}_i} a_{ij}\hat{\pi}_{\mu j} - \rho(t)\hat{m}_i + b_i\dot{\mu}_{0,l} \\ -\frac{1}{\mathcal{T}_s(1-\gamma)}\left\langle \frac{\mathrm{d}\hbar\left(\hat{E}_{\mu i}\right)}{\mathrm{d}\hat{E}_{\mu i}} \right\rangle^{-1} \circ \mathrm{sig}\left(\hbar\left(\hat{E}_{\mu i}\right)\right)^{\gamma} \end{array}\right], \end{cases} \tag{4.7}$$

where

$$\rho(t) = \frac{k_1}{2} + \frac{1}{k_2}\frac{\dot{\wp}\left(t, \mathcal{T}_e\right)}{\wp\left(t, \mathcal{T}_e\right)} \tag{4.8}$$

with $\mathcal{T}_e, k_1, k_2 > 0$, and $\wp, \dot{\wp}$ are as the same as that given in Lemma 2.

Next, it will further construct the MPLT algorithm based on the PDE algorithm. Before moving on, the following error vectors are defined as follows:

$$\hat{e}_{\eta i} = \eta_i - \hat{\eta}_i, \hat{e}_{\varpi i} = \varpi_i - \hat{\varpi}_i.$$

Later, according to Subsection 2.2, the sliding mode surface for the MPLT algorithm is constructed as

$$\hat{s}_i = \hbar\left(\hat{e}_{\eta i}\right) + \left[\mathcal{T}_{\bar{s}}\left(1 - \frac{\gamma_1}{\gamma_2}\right)\right]^{\frac{\gamma_2}{\gamma_1}} \mathrm{sig}\left(g\left(\hat{e}_{\eta i}, \hat{e}_{\varpi i}\right)\right)^{\frac{\gamma_2}{\gamma_1}}, \tag{4.9}$$

where $\mathcal{T}_{\bar{s}}, \gamma_1, \gamma_2$ are similarly defined as that in Eq (2.1), and $g\left(\hat{e}_{\eta_i}, \hat{e}_{\varpi i}\right)$ is a function that can be derived by replacing the term $\dot{\hat{e}}_{\eta i}$ as $\dot{\hat{e}}_{\varpi i}$ in the construction of $\dot{\hbar}(\hat{e}_{\eta i})$. In order to better illustrate the specific form of the designed MPLT algorithm, the time regulator function and its derivative are selected as

$$\hbar(x) = x/\sqrt{1+x^2},$$

and

$$\dot{\hbar}(x) = x/(1+x^2)^{-3/2}.$$

In this way, one has

$$\hbar\left(\hat{e}_{\eta i}\right) = \hat{e}_{\eta i} \circ \left\langle \mathbf{1} + \left\langle \hat{e}_{\eta i} \right\rangle^2 \right\rangle^{-1/2}, \tag{4.10}$$

$$g\left(\hat{e}_{\eta i}, \hat{e}_{\varpi i}\right) = \hat{e}_{\varpi i} \circ \left\langle \mathbf{1} + \left\langle \hat{e}_{\eta i} \right\rangle^2 \right\rangle^{-3/2}. \tag{4.11}$$

Then, the MPLT algorithm for the NMSVs is designed as

$$\begin{cases} \tau_i = R^T(\psi_i)\,\Xi_i \left(\left\langle \mathbf{1} + \left\langle \hat{e}_{\eta i} \right\rangle^2 \right\rangle^{\frac{3}{2}} \circ \left(\tau_{eq,i} + \tau_{s,i} \right) + \kappa\left(\hat{e}_{\eta i}\right) + \hat{\mu}_i + \tau_{f,i} \right), \\ \tau_{eq,i} = -\frac{\gamma_1}{\gamma_2 k_g} \mathrm{sig}\Big(g\left(\hat{e}_{\eta_i}, \hat{e}_{\varpi i}\right) \Big)^{2-\frac{\gamma_2}{\gamma_1}}, \\ \tau_{s,i} = -\dfrac{\gamma_1 \vartheta \Big(\alpha \left\| \hat{s}_i \right\|_1^{\rho} + \beta \left\| \hat{s}_i \right\|_1^{\ell} \Big)^k}{\gamma_2 k_g \mathcal{T}_c} \mathrm{diag}\left\{ \mu_{\varrho}\left(\left| g\Big(\hat{e}_{\eta_i}, \hat{e}_{\varpi i}\Big)^{\frac{\gamma_2}{\gamma_1 - 1}} \right| \right) \right\} \\ \qquad \times \mathrm{diag}\left\{ \left| g\left(\hat{e}_{\eta_i}, \hat{e}_{\varpi i}\right) \right|^{1-\frac{\gamma_2}{\gamma_1}} \right\} \mathrm{sgn}\left(\hat{s}_i\right) - k_f \mathrm{sgn}\left(\hat{s}_i\right), \\ \tau_{f,i} = -\hat{z}_i, \end{cases} \tag{4.12}$$

where Ξ_i is a designed symmetric positive-definite gain matrix. $\vartheta, \alpha, \beta, \rho, \ell, k$ are defined as the same as that in Lemma 1,

$$k_g = \left[\mathcal{T}_{\tilde{s}} \left(1 - \gamma_1/\gamma_2 \right) \right]^{\gamma_2/\gamma_1}, \ \mathcal{T}_c > 0$$

is the predefined-time parameter,

$$\kappa\left(\hat{e}_{\eta i}\right) = 3\hat{e}_{\eta i} \circ \langle \hat{e}_{\varpi i} \rangle^2 \circ \left\langle \mathbf{1} + \left\langle \hat{e}_{\eta i} \right\rangle^2 \right\rangle^{-1}, \ k_f > 0,$$

$$\mu_{\varrho}\left(\left| g\left(\hat{e}_{\eta_i}, \hat{e}_{\varpi i}\right) \right|^{\gamma_2/\gamma_1 - 1} \right) = \mathrm{col}\left(\left| g_k\left(\hat{e}_{\eta_i}, \hat{e}_{\varpi i}\right) \right|^{\gamma_2/\gamma_1 - 1} \right), \ k = \{1, 2, 3\},$$

here, and $g_k\left(\hat{e}_{\eta_i}, \hat{e}_{vi}\right)$ denote the kth element of $g\left(\hat{e}_{\eta_i}, \hat{e}_{vi}\right)$. $\hat{z}_i$ is governed by the following super-twisting observer:

$$\begin{cases} \dot{\hat{y}}_i = -\kappa_{1,i} \mathrm{sig}(\hat{y}_i - \hat{e}_{\varpi i})^{1/2} + \hat{z}_i - \hat{\mu}_i + \Xi_i^{-1} R(\psi_i)\,\tau_i, \\ \dot{\hat{z}}_i = -\kappa_{2,i} \mathrm{sgn}\left(\hat{y}_i - \hat{e}_{\varpi i}\right), \end{cases} \tag{4.13}$$

where $\kappa_{i,1}, \kappa_{i,2} > 0$.

Remark 2. *It is noteworthy that the model information, i.e., the dynamical matrices $\bar{M}_i(\eta_i), \bar{C}_i(\eta_i, \dot{\eta}_i), \bar{D}_i(\eta_i, \dot{\eta}_i)$ (or $M_i, C_i(v_i), D_i(v_i)$), has not been used in the constructed MPLT alogrithm. Thus, this means that the designed MPLT algorithm is model independent. All unknown model-dependent terms are lumped into the disturbance-like term Q_i, which is fully estimated in real time by the super-twisting observer.*

Remark 3. *The integral predefined-time sliding mode surface in the PDE estimator ensures strict convergence of coordination errors within a predefined time, while avoiding singularities in distributed systems with Laplacian coupling. The nonsingular predefined-time terminal sliding mode surface in the MPLT tracking layer provides faster convergence near the origin and guarantees predefined-time tracking without the risk of finite-escape singularities.*

5. Stability analysis

5.1. Analysis for the PDE algorithm

This section demonstrates that the designed PDE estimator is capable of achieving distributed estimation of the virtual leaders' position, velocity, and acceleration within a predefined time. The result is formally stated in the next theorem.

Theorem 1. *Given that Assumptions 1–3 hold, and employing the PDE algorithm (4.7), if $\mathcal{T}_s, \mathcal{T}_e > 0$, $0 < \gamma < 1$, and $k_1, k_2 > 0$, then the states of the virtual leaders can be tracked by the corresponding follower vehicles within a predefined time $\mathcal{T}_1 = \mathcal{T}_s + \mathcal{T}_e$, i.e., $\hat{\eta}_i = \eta_{0,l}$, $\hat{\varpi}_i = \varpi_{0,l}$, $\hat{\mu}_i = \mu_{0,l}$, $\forall i \in \mathcal{V}_l$, $l \in \{1, 2, \ldots, M_l\}$, for $t \geq \mathcal{T}_1$.*

Proof. Based on the construction of $\hat{\pi}_{\eta_i}$ in (4.7), it has

$$\sum_{j\in\mathcal{N}_i} a_{ij}\left(\hat{\pi}_{\eta i} - \hat{\pi}_{\eta j}\right) + b_i\hat{\pi}_{\eta i} = -\rho(t)\hat{\sigma}_i + b_i\varpi_{0,l} - \frac{1}{\mathcal{T}_s(1-\gamma)}\left\langle\frac{\mathrm{d}\hbar\left(\hat{E}_{\eta i}\right)}{\mathrm{d}\hat{E}_{\eta i}}\right\rangle^{-1} \circ \mathrm{sig}\left(\hbar\left(\hat{E}_{\eta i}\right)\right)^{\gamma}. \tag{5.1}$$

Later, since the NMSVs contains N vehicles, the compact vectors of the earlier defined variables are contructed as follows:

$$\begin{aligned}
\hat{\eta} &= \mathrm{col}\{\hat{\eta}_1, \hat{\eta}_2, \ldots, \hat{\eta}_N\}, \quad \hat{E}_\eta = \mathrm{col}\{\hat{E}_{\eta 1}, \hat{E}_{\eta 2}, \ldots, \hat{E}_{\eta N}\},\\
\hat{\sigma} &= \mathrm{col}\{\hat{\sigma}_1, \hat{\sigma}_2, \ldots, \hat{\sigma}_N\}, \quad \hat{\pi}_\eta = \mathrm{col}\{\hat{\pi}_{\eta 1}, \hat{\pi}_{\eta 2}, \ldots, \hat{\pi}_{\eta N}\},\\
\eta_0 &= \mathrm{col}\left(\mathbf{1}_{n_1}\otimes\eta_{0,1}, \mathbf{1}_{n_2}\otimes\eta_{0,2}, \ldots, \mathbf{1}_{n_M}\otimes\eta_{0,M}\right),\\
\varpi_0 &= \mathrm{col}\left(\mathbf{1}_{n_1}\otimes\varpi_{0,1}, \mathbf{1}_{n_2}\otimes\varpi_{0,2}, \ldots, \mathbf{1}_{n_M}\otimes\varpi_{0,M}\right),\\
\mu_0 &= \mathrm{col}\left(\mathbf{1}_{n_1}\otimes\mu_{0,1}, \mathbf{1}_{n_2}\otimes\mu_{0,2}, \ldots, \mathbf{1}_{n_M}\otimes\mu_{0,M}\right),
\end{aligned}$$

where $n_1, n_2, \ldots, n_M$ denote the vehicle number of each subgroup, $\tilde{\eta} = \hat{\eta} - \eta_0$. In this way, Eq (5.1) can be rewritten as following compact form:

$$\left[(\mathcal{L}+\mathcal{B})\otimes I_3\right]\hat{\pi}_\eta = -\rho(t)\hat{\sigma} + (\mathcal{B}\otimes I_3)\,\varpi_0 - \frac{1}{\mathcal{T}_s(1-\gamma)}\left\langle\frac{\mathrm{d}\hbar\left(\hat{E}_\eta\right)}{\mathrm{d}\hat{E}_\eta}\right\rangle^{-1} \circ \mathrm{sig}\left(\hbar\left(\hat{E}_\eta\right)\right)^{\gamma}. \tag{5.2}$$

On the other hand, it can be derived from the construction of $\hat{E}_{\eta i}$ and Assumption 2 that

$$\hat{E}_\eta = \left[(\mathcal{L}+\mathcal{B})\otimes I_3\right]\tilde{\eta}. \tag{5.3}$$

It then follows that

$$\begin{aligned}
\dot{\hat{E}}_\eta &= \left[(\mathcal{L}+\mathcal{B})\otimes I_3\right]\dot{\hat{\eta}}\\
&= \left[(\mathcal{L}+\mathcal{B})\otimes I_3\right](\hat{\pi}_\eta - \varpi_0)\\
&= -\rho(t)\hat{\sigma} - \frac{1}{\mathcal{T}_s(1-\gamma)}\left\langle\frac{\mathrm{d}\hbar\left(\hat{E}_\eta\right)}{\mathrm{d}\hat{E}_\eta}\right\rangle^{-1} \circ \mathrm{sig}\left(\hbar\left(\hat{E}_\eta\right)\right)^{\gamma},
\end{aligned} \tag{5.4}$$

since

$$[(\mathcal{L}+\mathcal{B})\otimes I_3]\,\varpi_0 = (\mathcal{B}\otimes I_3)\varpi_0.$$

Furthermore, according to (4.4), the compact expression of the designed sliding-mode vector $\hat{\sigma}_i$ can be formulated as

$$\hat{\sigma} = \hat{E}_\eta + \frac{1}{\mathcal{T}_s(1-\gamma)}\int_0^t \left\langle \frac{\mathrm{d}\hbar\left(\hat{E}_\eta(\sigma)\right)}{\mathrm{d}\hat{E}_\eta(\sigma)} \right\rangle^{-1} \circ \mathrm{sig}\Big(\hbar\left(\hat{E}_\eta(\sigma)\right)\Big)^\gamma \mathrm{d}\sigma. \tag{5.5}$$

Differentiating $\hat{\sigma}$ along (5.5) yields that

$$\dot{\hat{\sigma}} = -\rho(t)\hat{\sigma}. \tag{5.6}$$

Construct the Lyapunov function candidate for (5.6) as

$$V(\hat{\sigma}) = \frac{1}{2}\hat{\sigma}^T\hat{\sigma}.$$

It then follows that

$$\dot{V}(\hat{\sigma}) = -\left(\frac{k_1}{2} + \frac{1}{k_2}\frac{\dot{\wp}\,(t,\mathcal{T}_e)}{\wp\,(t,\mathcal{T}_e)}\right)\|\hat{\sigma}\|^2 \le -k_1 V(\hat{\sigma}) - \frac{2}{k_2}\frac{\dot{\wp}\,(t,\mathcal{T}_e)}{\wp\,(t,\mathcal{T}_e)}V(\hat{\sigma}). \tag{5.7}$$

Thus, according to Lemma 2, $\hat{\sigma}$ converges to the origin within a predefined time $t \le \mathcal{T}_e$. Based on the results of integral predefined-time sliding mode surface presented in Subsection 2.2, it can eventually conclude that $\hat{E}_\eta$ converges to the origin within a predefined time

$$t \le \mathcal{T}_e + \mathcal{T}_s.$$

Furthermore, Assumptions 1 and 2 grantee that $\mathcal{L}+\mathcal{B}$ is full rank, thus

$$\hat{E}_\eta = [(\mathcal{L}+\mathcal{B})\otimes I_3]\,\tilde{\eta} = \mathbf{0}$$

implies that $\tilde{\eta} = \mathbf{0}$, namely, the position estimator error $\tilde{\eta}$ would converge to the origin within a predefined time

$$t \le \mathcal{T}_1 \triangleq \mathcal{T}_e + \mathcal{T}_s,$$

i.e., $\hat{\eta}_i = \eta_{0,l}$ for $t \ge \mathcal{T}_1$, $\forall i \in \mathcal{V}_l$, $l \in \{1,2,\ldots,M_l\}$. Later, with similar stability analysis, it has

$$\hat{\varpi}_i = \varpi_{0,l} \ \text{ and } \ \hat{\mu}_i = \mu_{0,l}$$

for $t \ge \mathcal{T}_1$, $\forall i \in \mathcal{V}_l$, $l \in \{1,2,\ldots,M_l\}$. This completes the proof. □

5.2. Analysis for the MPLT algorithm

This section proceeds to investigate the closed-loop stability under the designed MPLT algorithm. With the introduction of the symmetric positive-definite matrix Ξ_i, the model given in (3.2) is equivalently expressed as

$$\begin{cases} \dot{\eta}_i = \varpi_i, \\ \dot{\varpi}_i = \mathcal{Q}_i + \Xi_i^{-1}R_i\,(\psi_i)\,\tau_i, \\ \mathcal{Q}_i = \Xi_i^{-1}\left\{\bar{M}_i d_i(t) - \left[\left(\bar{M}_i - \Xi_i\right)\dot{\varpi}_i + \bar{C}_i\dot{\eta}_i + \bar{D}_i\dot{\eta}_i\right]\right\}, \end{cases} \tag{5.8}$$

where $\bar{M}_i$, $\bar{C}_i$, and $\bar{D}_i$ are the abbreviations of $\bar{M}_i\,(\eta_i)$, $\bar{C}_i\,(\eta_i,\dot{\eta}_i)$, and $\bar{D}_i\,(\eta_i,\dot{\eta}_i)$. Further, a reasonable assumption on $\mathcal{Q}_i$ is given as follows.

Assumption 4. *For all $i \in \mathcal{V}$, the derivative of the dynamic term $\mathcal{Q}_i$ is uniformly bounded, i.e., there exists a positive constant $\zeta_{\mathcal{Q}}$ satisfying $\|\dot{\mathcal{Q}}_i\| \leq \zeta_{\mathcal{Q}}$.*

With the above setting, the corresponding derived results of the MPLT algorithm are presented in the following theorem.

Theorem 2. *Suppose that Assumptions 1–4 hold. Employing the MPLT algorithm (4.12) for NMSVs, if $\mathcal{T}_{\tilde{s}}, \mathcal{T}_c > 0$ satisfy*

$$\mathcal{T}_{\tilde{s}} + \mathcal{T}_c > \mathcal{T}_{obse},$$

and γ_1, γ_2 are positive odd integers such that $\gamma_1 < \gamma_2 < 2\gamma_1$, $\kappa_{1,i} \geq 1.5\sqrt{\zeta_{\mathcal{Q}}}$, $\kappa_{2,i} \geq 1.1\zeta_{\mathcal{Q}}$, and $k_f > 0$, then the multi-target tracking problem can be solved within a predefined time

$$\mathcal{T}_f = \mathcal{T}_1 + \mathcal{T}_2,$$

where

$$\mathcal{T}_2 = \mathcal{T}_{obse} + \mathcal{T}_{\tilde{s}} + \mathcal{T}_c + \epsilon(\varrho),$$

with $\mathcal{T}_{obse}$ being the settling time of the super-twisting observer and

$$\epsilon(\varrho) = \frac{2\varrho^{\frac{\gamma_1}{\gamma_2-\gamma_1}}}{k_f}.$$

In this way, the predefined time can be set within the permissible range $[\mathcal{T}_{obse}, +\infty)$.

Proof. In order to facilitate the subsequent stability analysis, (5.8) is further rewritten as the following error form:

$$\begin{cases} \dot{\hat{e}}_{\eta i} = \hat{e}_{\varpi i} - \dot{\hat{\eta}}_i + \dot{\hat{\varpi}}_i, \\ \dot{\hat{e}}_{\varpi i} = \mathcal{Q}_i + \Xi_i^{-1} R_i(\psi_i)\tau_i - \dot{\hat{\varpi}}_i. \end{cases} \tag{5.9}$$

First, the stability of the proposed super-twisting observer (4.13) is analyzed. Construct the observer error vectors

$$\tilde{y}_i = \hat{y}_i - \hat{e}_{\varpi i} \text{ and } \tilde{z}_i = \hat{z}_i - \mathcal{Q}_i.$$

By applying the relation in (5.10), the system described in (4.13) can be rewritten in the following error representation:

$$\begin{cases} \dot{\tilde{y}}_i = -\kappa_{1,i}\mathrm{sig}(\tilde{y}_i)^{\frac{1}{2}} + \tilde{z}_i - \hat{\mu}_i + \dot{\hat{\varpi}}_i, \\ \dot{\tilde{z}}_i = -\kappa_{2,i}\mathrm{sgn}(\tilde{y}_i) - \dot{\mathcal{Q}}_i. \end{cases} \tag{5.10}$$

For $t \geq \mathcal{T}_1$, Theorem 1 implies that $\hat{\varpi}_i = \varpi_{0,l}$, $\hat{\mu}_i = \mu_{0,l}$, $\forall i \in \mathcal{V}_l$, $l \in \{1, 2, \ldots, M_l\}$. This means that $\dot{\hat{\varpi}}_i = \hat{\mu}_i$ when $t \geq \mathcal{T}_1$. Thus, for $t \geq \mathcal{T}_1$, (5.10) equals to

$$\begin{cases} \dot{\tilde{y}}_i = -\kappa_{1,i}\mathrm{sig}(\tilde{y}_i)^{\frac{1}{2}} + \tilde{z}_i, \\ \dot{\tilde{z}}_i = -\kappa_{2,i}\mathrm{sgn}(\tilde{y}_i) - \dot{\mathcal{Q}}_i. \end{cases} \tag{5.11}$$

Further, according to Lemma 3 and Assumption 4, it follows that $\tilde{z}_i$ converges to the origin within $t \leq \mathcal{T}_1 + \mathcal{T}_{obse}$, namely, for $t \geq \mathcal{T}_1 + \mathcal{T}_{obse}$, $\hat{z}_i = \mathcal{Q}_i$, $\forall i \in \mathcal{V}_l$, $l \in \{1, 2, \ldots, M_l\}$.

Conversely, for $t \geq \mathcal{T}_1 + \mathcal{T}_{obser}$, (5.9) turns to be

$$\begin{cases} \dot{\hat{e}}_{\eta i} = \hat{e}_{\varpi i}, \\ \dot{\hat{e}}_{\varpi i} = \mathcal{Q}_i + \Xi_i^{-1} R_i(\psi_i)\tau_i - \hat{\mu}_i. \end{cases} \tag{5.12}$$

It can be derived from $\dot{\hat{e}}_{\eta i} = \hat{e}_{\varpi i}$ that

$$g\left(\hat{e}_{\eta i}, \hat{e}_{\varpi i}\right) = \dot{\hbar}\left(\hat{e}_{\eta i}\right),$$

and the constructed sliding mode vector $\hat{s}_i$ in (4.9) becomes

$$\hat{s}_i = \hbar\left(\hat{e}_{\eta i}\right) + \left[\mathcal{T}_{\tilde{s}}\left(1 - \frac{\gamma_1}{\gamma_2}\right)\right]^{\frac{\gamma_2}{\gamma_1}} \operatorname{sig}\left(\dot{\hbar}(\hat{e}_{\eta i})\right)^{\frac{\gamma_2}{\gamma_1}}. \tag{5.13}$$

Submitting the constructed MPLT algorithm (4.12) into (5.12) yields the following closed-loop system:

$$\begin{cases} \dot{\hat{e}}_{\eta i} = \hat{e}_{\varpi i}, \\ \dot{\hat{e}}_{\varpi i} = \left\langle \mathbf{1} + \left\langle \hat{e}_{\eta i} \right\rangle^2 \right\rangle^{\frac{3}{2}} \circ \left(\tau_{eq,i} + \tau_{s,i}\right) + \kappa\left(\hat{e}_{\eta i}\right) \\ \quad = \kappa\left(\hat{e}_{\eta i}\right) - \left\langle \mathbf{1} + \left\langle \hat{e}_{\eta i} \right\rangle^2 \right\rangle^{\frac{3}{2}} \circ \left[\frac{\gamma_1}{\gamma_2 k_g} \operatorname{sig}\left(\dot{\hbar}\left(\hat{e}_{\eta i}\right)\right)^{2-\frac{\gamma_2}{\gamma_1}} \right. \\ \qquad + \frac{\gamma_1 \vartheta\left(\alpha \|\hat{s}_i\|_1^{\rho} + \beta \|\hat{s}_i\|_1^{\ell}\right)^k}{\gamma_2 k_g \mathcal{T}_c} \operatorname{diag}\left\{\mu_{\varrho}\left(\left|\dot{\hbar}\left(\hat{e}_{\eta i}\right)^{\frac{\gamma_2}{\gamma_1}-1}\right|\right)\right\} \\ \qquad \left. \times \operatorname{diag}\left\{\left|\dot{\hbar}\left(\hat{e}_{\eta i}\right)\right|^{1-\frac{\gamma_2}{\gamma_1}}\right\} \operatorname{sgn}(\hat{s}_i) + k_f \operatorname{sgn}(\hat{s}_i) \right]. \end{cases} \tag{5.14}$$

Then differentiating $\hat{s}_i$ in (5.13) along (5.14) yields that

$$\dot{\hat{s}}_i = -\frac{\vartheta\left(\alpha \|\hat{s}_i\|_1^{\rho} + \beta \|\hat{s}_i\|_1^{\ell}\right)^k}{\mathcal{T}_c} \operatorname{diag}\left\{\mu_{\varrho}\left(\left|\dot{\hbar}\left(\hat{e}_{\eta i}\right)\right|^{\frac{\gamma_2}{\gamma_1}-1}\right)\right\} \operatorname{sgn}(\hat{s}_i) - \frac{\gamma_2 k_g k_f}{\gamma_1} \operatorname{diag}\left\{\left|\dot{\hbar}\left(\hat{e}_{\eta i}\right)\right|^{\frac{\gamma_2}{\gamma_1}-1}\right\} \operatorname{sgn}(\hat{s}_i). \tag{5.15}$$

Construct the Lyapunov function candidate for (5.15) as $V_i(\hat{s}_i) = \operatorname{sgn}^T(\hat{s}_i)\hat{s}_i$. It then follows that

$$\begin{aligned} \mathcal{D}^+ V_i(\hat{s}_i) =& \operatorname{sgn}^T(\hat{s}_i)\, \dot{\hat{s}}_i \\ \leq& -\frac{\vartheta}{\mathcal{T}_c} \lambda_{\min}\left(\operatorname{diag}\left\{\mu_{\varrho}\right\}\right)\left(\alpha \|\hat{s}_i\|_1^{\rho} + \beta \|\hat{s}_i\|_1^{\ell}\right)^k - \frac{\gamma_2 k_g k_f}{\gamma_1} \min_{k=1}^{3}\left\{\left|\dot{\hbar}_{ik}\right|^{\frac{\gamma_2}{\gamma_1}-1}\right\} \\ \leq& -\frac{\vartheta}{\mathcal{T}_c} \lambda_{\min}\left(\operatorname{diag}\left\{\mu_{\varrho}\right\}\right)\left(\|\hat{s}_i\|_1^{\rho} + \beta \|\hat{s}_i\|_1^{\ell}\right)^k \\ =& -\frac{\vartheta}{\mathcal{T}_c} \lambda_{\min}\left(\operatorname{diag}\left\{\mu_{\varrho}\right\}\right)\left(\alpha V_i^{\rho}(\hat{s}_i) + \beta V_i^{\ell}(\hat{s}_i)\right)^k, \end{aligned} \tag{5.16}$$

where $\dot{\hbar}_{ik}$ is the kth element of $\dot{\hbar}\left(\hat{e}_{\eta i}\right)$, and μ_{ϱ} is the abbreviation of $\mu_{\varrho}\left(\left|\hat{e}_{\eta i}\right|^{\gamma_2/\gamma_1 - 1}\right)$. For the sub-closed-loop dynamics in each dimension, by employing the phase-diagram partition and stability analysis approach presented in [32, Theorem 2], one obtains that $\hat{s}_i$ reaches the origin within a predefined settling time $\mathcal{T}_1 + \mathcal{T}_{\text{obse}} + \mathcal{T}_c + \epsilon(\varrho)$, where the term $\epsilon(\varrho)$ is specified in Theorem 2. Based on the results

of predefined-time sliding mode surface presented in Subsection 2.2, it has $\hat{e}_{\eta i}$ and $\hat{e}_{\varpi i}$ converge to the origin within predefined time

$$t \leq \mathcal{T}_1 + \mathcal{T}_{obse} + \mathcal{T}_c + \mathcal{T}_{\tilde{s}} + \epsilon(\varrho) = \mathcal{T}_1 + \mathcal{T}_2.$$

Finally, consider that

$$e_{\eta i} = \eta_i - \eta_{0,l} = \hat{e}_{\eta i} + \tilde{\eta}_i$$

and

$$e_{\varpi i} = \varpi_i - \varpi_{0,l} = \hat{e}_{\varpi i} + \tilde{\varpi}_i.$$

Based on the main results obtained in Theorems 1 and 2, it eventually obtains that $e_{\eta i}$ and $e_{\varpi i}$ converge to the origin within predefined time $t \leq \mathcal{T}_1 + \mathcal{T}_2$. This completes the proof. □

Remark 4. *It is noteworthy that although the fixed time $\epsilon(\varrho)$ for passing the potential areas where singularity problems may occur (derived by the phase diagram segmentation method in [32]) would have negative impacts on the predefined-time stability at the theoretical level, in practical application, one can select a small parameter ϱ such that $\epsilon(\varrho)$ is small enough and can be neglected, since $\epsilon(\varrho)$ is inversely proportional to ϱ.*

Remark 5. *Note that the observer process and the tracking process are running simultaneously. Thus, in fact, as long as*

$$\mathcal{T}_c + \mathcal{T}_{\tilde{s}} + \epsilon(\varrho) > \mathcal{T}_{obse},$$

the settling time of the MPLT algorithm turns to be

$$\mathcal{T}_2 = T_c + \mathcal{T}_{\tilde{s}} + \epsilon(\varrho).$$

This implies that $\mathcal{T}_{obse}$ could be neglected if $\mathcal{T}_2$ is selected in the range $[\mathcal{T}_1 + \mathcal{T}_{obse}, +\infty]$.

Remark 6. *It can be found from the controller design that such predefined-time algorithm is essentially designed based on the finite-time terminal sliding mode control method. Thus, the computational complexity of the proposed controller is less than the fixed-time ones, since the fixed-time scheme involves a more complex coupling design structure.*

Remark 7. *Although predefined-time control ensures convergence within a user-defined time, it may cause the control input to become excessively large as the system approaches the predefined time. This is particularly true when the predefined-time parameter $\mathcal{T}_{per}$ is small, leading to high control effort in order to guarantee convergence. Thus, for guaranteeing the onboard implementation feasibility of the proposed scheme, the predefined-time parameters should be selected in a proper way. Besides, future work could explore adaptive mechanisms to adjust $\mathcal{T}_{per}$ to keep the control effort within acceptable limits while ensuring predefined-time convergence.*

Remark 8. *The main motivation for using predefined-time control is to ensure that the system converges to the desired state within a fixed-time interval. In many real-world applications, especially for systems like NMSVs, it is critical to meet strict timing requirements, such as completing a mission within a specific time window due to operational constraints like environmental conditions, safety considerations, or mission scheduling. Predefined-time control guarantees convergence within the specified time regardless of initial conditions, making it particularly useful for applications with stringent time constraints.*

6. Simulation examples

Example 1. This section considers 11 CyberShip II vessels forming the NMSV network, which is organized into three cooperative subgroups. The designed control scheme is performed on such NMSVs to verify its effectiveness.

Simulation settings. In the simulation example, the communication topology is constructed as is shown in Figure 2 according to Assumptions 1 and 2. Besides, the physical parameters and the specific constructions of the dynamical terms can be referred to [33].

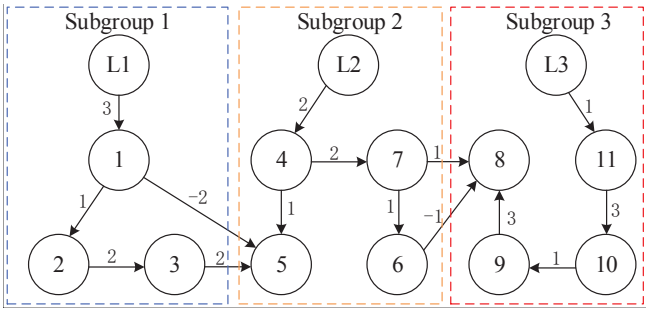

Figure 2. The interaction topology of the NMSVs in the simulation example.

With respect to the group division of the NMSVs, three virtual leaders are involved in the simulation example. Without loss of generality, considering Assumption 3, the motion trajectories of the leaders expressed in the earth-fixed coordinates are specified as follows:

$$\begin{cases} \eta_{0,1} = [-5 + 5\sin(0.3t), 3 - 5\cos(0.3t), 0.3t]^T, \\ \varpi_{0,1} = [1.5\cos(0.3t), 1.5\sin(0.3t), 0.3]^T, \\ \mu_{0,1} = [-0.45\sin(0.3t), 0.45\cos(0.3t), 0]^T, \end{cases}$$

$$\begin{cases} \eta_{0,2} = [3 + 3\sin(0.5t), 3 + 3\cos(0.5t), -0.5t]^T, \\ \varpi_{0,2} = [1.5\cos(0.5t), -1.5\sin(0.5t), -0.5]^T, \\ \mu_{0,2} = [-0.75\sin(0.7t), -0.75\cos(0.5t), 0]^T, \end{cases}$$

$$\begin{cases} \eta_{0,3} = [3 + 4\sin(0.4t), -7 - 4\cos(0.4t), 0.4t]^T, \\ \varpi_{0,3} = [1.6\cos(0.4t), 1.6\sin(0.4t), 0.4]^T, \\ \mu_{0,3} = [-0.64\sin(0.4t), 0.64\cos(0.4t), 0]^T. \end{cases}$$

Control parameter settings. According to the sufficient conditions established in Theorem 1, the control parameters of the PDE algorithm are chosen as

$$\mathcal{T}_s = 0.5, \ \mathcal{T}_e = 0.5, \ k_1 = 1, \ k_2 = 1, \ \text{and} \ \gamma = 0.5.$$

The time-regulation function is specified as

$$\hbar(x) = x/\sqrt{1 + x^2}.$$

Subsequently, based on the sufficient conditions provided in Theorem 2, the parameters of the MPLT algorithm are set to

$$\mathcal{T}_{\tilde{s}} = 3, \ \mathcal{T}_c = 4, \ \gamma_1 = 3, \ \gamma_2 = 5, \ \varrho = 0.001, \ k_f = 0.01, \ \alpha = 0.1, \ \beta = 0.4, \ \rho = 0.8, \ \ell = 3 \ \text{and}, \ k = 0.6.$$

The observer gains are further selected as

$$\kappa_{1,i} = 1.5\sqrt{10000}$$

and

$$\kappa_{2,i} = 10000.$$

Example 1 results. The simulation results are presented in Figures 3–7. Figure 3 shows that $\hat{\eta}_i$ can track the corresponding virtual leader, and the tracking error $\tilde{\eta}_i$ is forced to the origin within the set predefined time

$$t \leq \mathcal{T}_1 = \mathcal{T}_s + \mathcal{T}_e = 1.$$

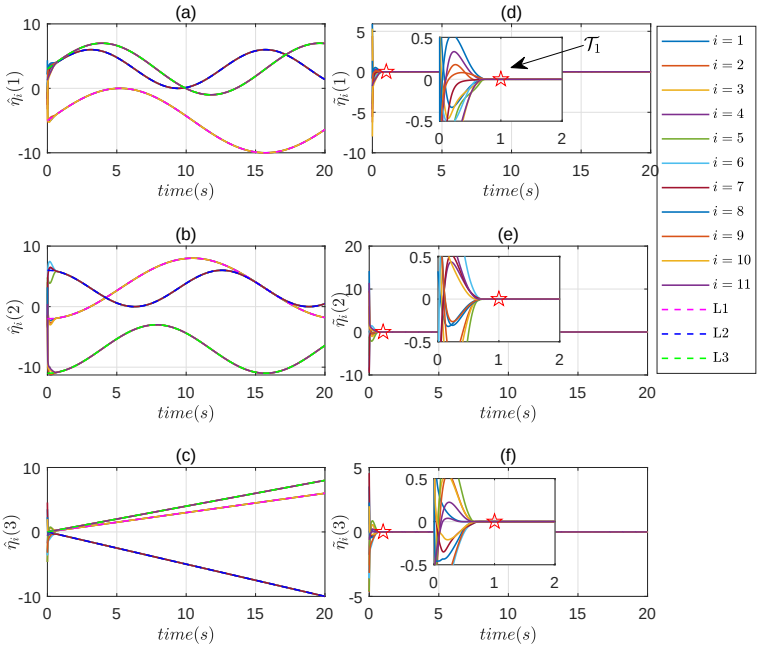

Figure 3. (a)–(c) depict the evolution of $\hat{\eta}_i$ for coordinates 1–3; (d)–(f) depict the evolution of $\tilde{\eta}_i$ for coordinates 1–3.

Besides, Figures 4 and 5 show the same conclusion on the estimators $\hat{\varpi}_i$ and $\hat{\mu}_i$. This thus totally shows the effectiveness of the designed PDE algorithm. Further, Figures 6 and 7 give the evolutions of the states η_i and ϖ_i, as well as the tracking errors $e_{\eta i}$ and $e_{\varpi i}$, from which it can be observed that tracking errors can also converge to the origin within the selected predefined time, and then successfully address the considered multi-target tracking problem. Thus, it can be concluded that the designed PDE and MPLT algorithms are of great predefined-time performance when they actuates the NMSVs in a model-independent way.

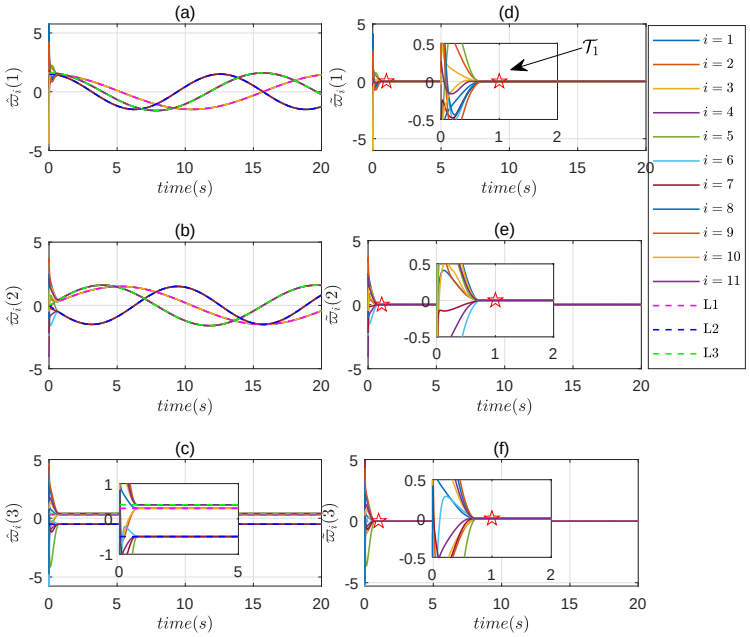

Figure 4. (a)–(c) depict the evolution of $\hat{\varpi}_i$ for coordinates 1–3; (d)–(f) depict the evolution of $\tilde{\varpi}_i$ for coordinates 1–3.

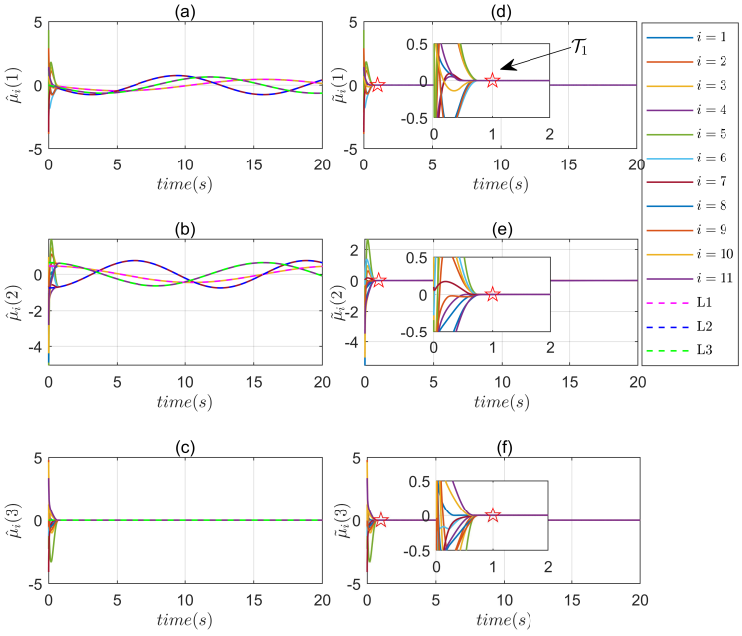

Figure 5. (a)–(c) depict the evolution of $\hat{\mu}_i$ for coordinates 1–3; (d)–(f) depict the evolution of $\tilde{\mu}_i$ for coordinates 1–3.

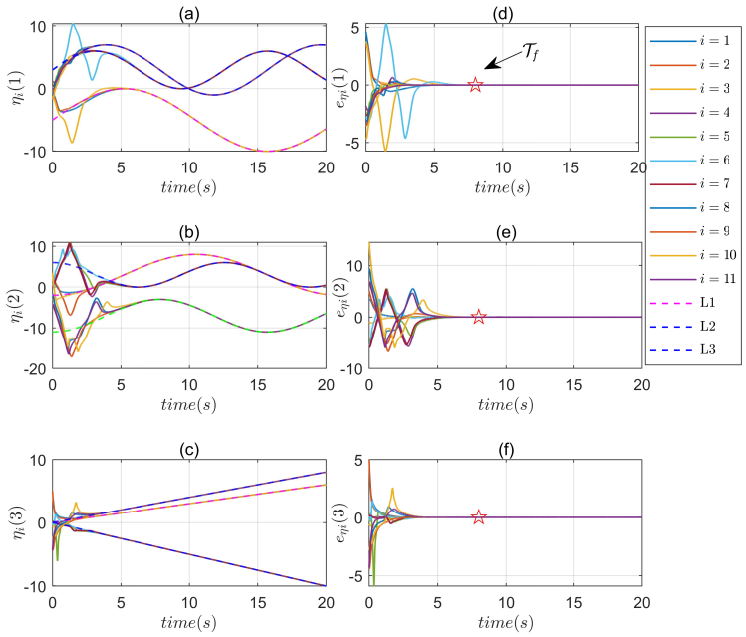

Figure 6. (a)–(c) depict the evolution of η_i for coordinates 1–3; (d)–(f) depict the evolution of $e_{\eta i}$ for coordinates 1–3.

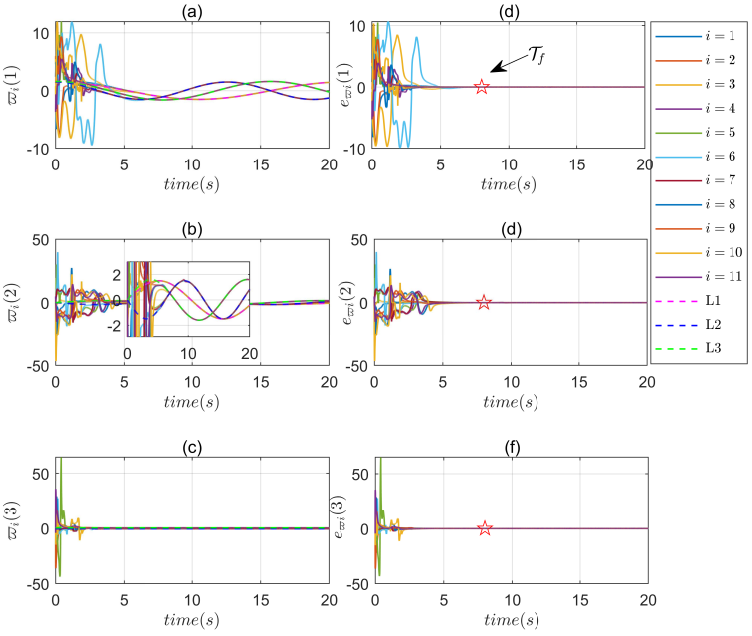

Figure 7. (a)–(c) depict the evolution of ϖ_i for coordinates 1–3; (d)–(f) depict the evolution of $e_{\varpi i}$ for coordinates 1–3.

Example 2. A comparative experiment has been performed to evaluate the proposed MPLT algorithm against the local fixed-time controller algorithm presented in [38]. In this experiment, both algorithms were tested under the same model used in Example 1. For the MPLT algorithm, in Example 2, the values of $\mathcal{T}_{\tilde{s}}$ and $\mathcal{T}_c$ that were set are $\mathcal{T}_{\tilde{s}} = 3$, $\mathcal{T}_c = 4$. For the local fixed-time controller algorithm, the control parameter settings are the same as those in the [38]. The settings of other variables (initial state, model parameters, leader trajectory, etc.) are the same as in Example 1.

Example 2 results. Figure 8 shows the convergence speeds of the two algorithms. It is obvious that the algorithm in this paper converges more quickly.

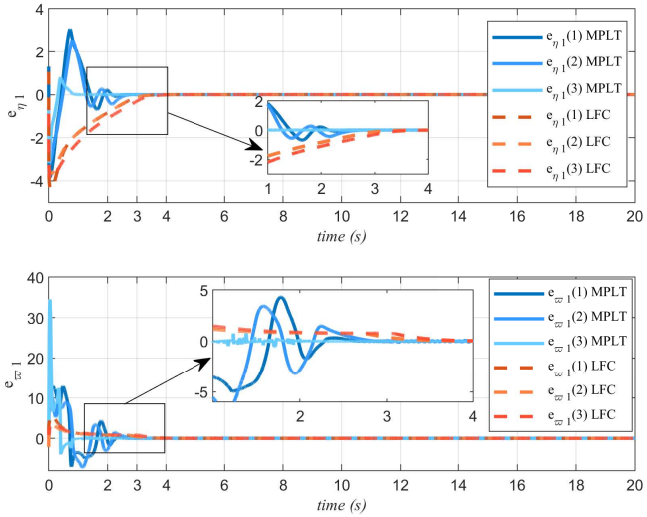

Figure 8. The convergence speeds of the two algorithms in Example 2.

7. Conclusions

This paper has successfully addressed the model-independent multi-target tracking problem of the NMSVs within a predefined time by constructing a hierarchical control scheme, which is built by the PDE algorithm and the MPLT algorithm. By using the PDE algorithm, the states of the leaders can be precisely estimated in a distributed way within a predefined time, which thus helps all the vehicles gain the information of their corresponding leaders. Later, the MPLT algorithm addresses the considered problem based on the obtained estimators. Besides, the sufficient conditions have been given through systematic Lyapunov stability analysis. Finally, the derived simulation results verify the correctness and the effectiveness of the designed control scheme. In future work, we plan to investigate more robust communication models, including time-varying and switching topologies, as well as strategies to handle packet loss and communication delays in real-world maritime networks.

Author contributions

Xionghua Liu: writing-original draft, methodology, funding acquisition; Yang Zhang: writing-original draft, writing-review and editing; Kai-Lun Huang: methodology, writing-review and

editing, funding acquisition; Jing-Zhe Xu: writing-review and editing, validation, funding acquisition; Chang-Duo Liang: writing-review and editing, conceptualization, supervision, funding acquisition. All authors have read and approved the final version of the manuscript for publication.

Use of Generative-AI tools declaration

ChatGPT was used to improve the language and readability of this article. The authors reviewed and edited the content and take full responsibility for the final version.

Acknowledgments

This work was supported by the National Natural Science Foundation of China under Grants 62403187, 624B2055, in part by the Natural Science Foundation of Hubei Province of China under Grant 2025AFB182, in part by Hubei Provincial Department of Education Research Project under Grant B2023316, in part by Special Fund of Advantageous and Characteristic Disciplines (Group) of Hubei Province, in part by China Higher Education Association "2023 Higher Education Scientific Research Project", Grant Number: 23XXK0403, in part by 2023 Philosophy and Social Science Research Project of Hubei Provincial Department of Education under Grant 23G130, in part by the Scientific Research Team Plan of Wuhan Technology and Business University under Grants WPT2023055, WZT2025003, and in part by the University-level Scientific Research Projects of Wuhan Technology and Business University under Grant D2025001.

Conflict of interest

The authors declare that there are no conflicts of interest.

References

1. Y. Qiao, J. Yin, W. Wang, F. Duarte, J. Yang, C. Ratti, Survey of deep learning for autonomous surface vehicles in marine environments, *IEEE Trans. Intell. Transp. Syst.*, **24** (2023), 3678–3701. https://doi.org/10.1109/TITS.2023.3235911
2. R. Pellegrini, S. Ficini, A. Odetti, A. Serani, M. Caccia, M. Diez, Multi-fidelity hydrodynamic analysis of an autonomous surface vehicle at surveying speed in deep water subject to variable payload, *Ocean Eng.*, **271** (2023), 113529. https://doi.org/10.1016/j.oceaneng.2022.113529
3. J. P. Martinez-Esteso, F. J. Castellanos, A. Rosello, J. Calvo-Zaragoza, A. J. Gallego, On the use of synthetic data for body detection in maritime search and rescue operations, *Eng. Appl. Artif. Intell.*, **139** (2025), 109586. https://doi.org/10.1016/j.engappai.2024.109586
4. J. Li, Y. Zhang, H. W. J. Lee, Y. Wang, Fuzzy tracking control of singular multi-agent systems under switching topology, *AIMS Math.*, **9** (2024), 29718–29735. https://doi.org/10.3934/math.20241440
5. X. Gong, Z. Zhang, Y. Cui, S. Liang, Observer-based secure consensus tracking of positive multi-agent systems under periodic denial-of-service attacks, *J. Franklin Inst.*, **361** (2024), 106716. https://doi.org/10.1016/j.jfranklin.2024.106716

6. X. Wu, S. Ding, H. Wang, N. Xu, X. Zhao, W. Wang, Dual-channel event-triggered prescribed performance adaptive fuzzy time-varying formation tracking control for nonlinear multi-agent systems, *Fuzzy Sets Syst.*, **498** (2025), 109140. https://doi.org/10.1016/j.fss.2024.109140
7. Z. Feng, G. Hu, X. Dong, J. Lu, Discrete-time adaptive distributed output observer for time-varying formation tracking of heterogeneous multi-agent systems, *Automatica*, **160** (2024), 111400. https://doi.org/10.1016/j.automatica.2023.111400
8. L. Shi, Z. Ma, S. Yan, T. Ao, Flocking dynamics for cooperation-antagonism multi-agent networks subject to limited communication resources, *IEEE Trans. Circuits Syst. I*, **71** (2024), 1396–1405. https://doi.org/10.1109/TCSI.2023.3347073
9. O. Artime, M. Grassia, M. D. Domenico, J. P. Gleeson, H. A. Makse, G. Mangioni, et al., Robustness and resilience of complex networks, *Nat. Rev. Phys.*, **6** (2024), 114–131.
10. Y. Li, W. Du, P. Yang, T. Wu, J. Zhang, D. Wu, et al., A satisficing conflict resolution approach for multiple UAVs, *IEEE Int. Things J.*, **6** (2019), 1866–1878. https://doi.org/10.1109/JIOT.2018.2885147
11. D. Zeng, B. Zeng, Y. Liu, J. Zhao, C. Cai, Practical prescribed-time trajectory tracking control for marine surface vehicles, *IEEE Trans. Circuits and Syst. II*, **71** (2024), 4899–4903. https://doi.org/10.1109/TCSII.2024.3410466
12. J. Ning, Y. Wang, E. Wang, L. Liu, C. P. Chen, S. Tong, Fuzzy trajectory tracking control of under-actuated unmanned surface vehicles with ocean current and input quantization, *IEEE Trans. Syst. Man Cybern.*, **55** (2025), 63–72. https://doi.org/10.1109/TSMC.2024.3460370
13. X. Hu, Y. Xiong, Z. Zhang, C. Li, Consensus of a new multi-agent system via multi-task, multi-control mechanism and multi-consensus strategy, *Neurocomputing*, **584** (2024), 127586. https://doi.org/10.1016/j.neucom.2024.127586
14. F. Cacace, M. Mattioni, S. Monaco, D. Normand-Cyrot, Consensus and multi-consensus for discrete-time LTI systems, *Automatica*, **166** (2024), 111718. https://doi.org/10.1016/j.automatica.2024.111718
15. Y. Huang, X. Xiang, C. Yan, H. Xu, T. Hu, H. Zhou, Self-organized multitarget pursuit in multi-unmanned aerial vehicle systems via hierarchical probabilistic graphical models, *Adv. Intell. Syst.*, **7** (2025), 2401110. https://doi.org/10.1002/aisy.202401110
16. H. V. Nguyen, B. N. Vo, B. T. Vo, H. Rezatofighi, D. C. Ranasinghe, Multi-objective multi-agent planning for discovering and tracking multiple mobile objects, *IEEE Trans. Signal Process.*, **72** (2024), 3669–3685. https://doi.org/10.1109/TSP.2024.3423755
17. J. Li, T. Han, B. Xiao, Q. Yang, H. Yan, Observer-based time-varying group formation tracking for one-sided Lipschitz nonlinear second-order multi-agent systems, *Trans. Inst. Meas. Control*, **45** (2023), 3011–3019. https://doi.org/10.1177/01423312231162896
18. Y. Wang, Z. Wang, H. Zhang, H. Yan, Group formation tracking of heterogeneous multi-agent systems using reinforcement learning, *IEEE Trans. Control Network Syst.*, **12** (2025), 497–509. https://doi.org/10.1109/TCNS.2024.3487653
19. K. L. Huang, C. D. Liang, X. Zhan, T. Han, L. Yan, M. F. Ge, Bipartite formation-containment of networked marine surface vehicles via hierarchical finite-time fuzzy control scheme, *IEEE Trans. Veh. Technol.*, 2025. https://doi.org/10.1109/TVT.2025.3610078

20. Y. Zhu, J. Zhang, L. Chen, X. Chen, C. Y. Su, Learning observer based fault estimation for a class of unmanned marine vehicles: The switched system approach, *IEEE Trans. Autom. Sci. Eng.*, **21** (2024), 5665–5676. https://doi.org/10.1109/TASE.2023.3314757

21. J. Qin, J. Du, J. Li, Adaptive finite-time trajectory tracking event-triggered control scheme for underactuated surface vessels subject to input saturation, *IEEE Trans. Intell. Transp. Syst.*, **24** (2023), 8809–8819. https://doi.org/10.1109/TITS.2023.3256094

22. J. Ning, Y. Wang, C. P. Chen, T. Li, Neural network observer based adaptive trajectory tracking control strategy of unmanned surface vehicle with event-triggered mechanisms and signal quantization, *IEEE Trans. Emerging Top. Comput. Intell.*, **9** (2025), 3136–3146. https://doi.org/10.1109/TETCI.2025.3526333

23. Z. Peng, Y. Jiang, L. Liu, Y. Shi, Path-guided model-free flocking control of unmanned surface vehicles based on concurrent learning extended state observers, *IEEE Trans. Syst. Man Cybern.*, **53** (2023), 4729–4739. https://doi.org/10.1109/TSMC.2023.3256371

24. H. Y. Park, J. H. Kim, Model-free control approach to uncertain Euler-Lagrange equations with a Lyapunov-based L_∞-gain analysis, *AIMS Math.*, **8** (2023), 17666–17686. https://doi.org/10.3934/math.2023902

25. E. A. Basso, H. M. Schmidt-Didlaukies, K. Y. Pettersen, A. J. Sorensen, Global asymptotic tracking for marine vehicles using adaptive hybrid feedback, *Trans. Automa. Control*, **68** (2022), 1584–1599. https://doi.org/10.1109/TAC.2022.3161372

26. D. Zhang, H. Chen, Q. Lu, C. Deng, G. Feng, Finite-time cooperative output regulation of heterogeneous nonlinear multi-agent systems under switching DoS attacks, *Automatica*, **173** (2025), 112062. https://doi.org/10.1016/j.automatica.2024.112062

27. J. Zhang, S. Yu, Y. Yan, Y. Zhao, Fixed-time sliding mode trajectory tracking control for marine surface vessels with input saturation and prescribed performance constraints, *Nonlinear Dyn.*, **112** (2024), 17169–17181. https://doi.org/10.1007/s11071-024-09918-9

28. X. Yue, H. Zhang, J. Ma, Predefined-time safe cooperative control for multiagent systems with privacy preservation and unknown disturbances, *IEEE Trans. Cybern.*, 2025. https://doi.org/10.1109/TCYB.2025.3611950

29. H. Wang, Q. Liu, J. H. Park, Predefined-time fuzzy adaptive optimal secure consensus control for multi-agent systems with unknown follower dynamics, *IEEE Trans. Fuzzy Syst.*, **33** (2025), 2122–2135. https://doi.org/10.1109/TFUZZ.2025.3552050

30. J. X. Zhang, T. Chai, Singularity-free continuous adaptive control of uncertain underactuated surface vessels with prescribed performance, *IEEE Trans. Syst. Man Cybern.*, **52** (2022), 5646–5655. https://doi.org/10.1109/TSMC.2021.3129798

31. J. X. Zhang, T. Yang, T. Chai, Neural network control of underactuated surface vehicles with prescribed trajectory tracking performance, *IEEE Trans. Neural Networks Learn. Syst.*, **35** (2024), 8026–8039. https://doi.org/10.1109/TNNLS.2022.3223666

32. C. D. Liang, M. F. Ge, Z. W. Liu, G. Ling, X. W. Zhao, A novel sliding surface design for predefined-time stabilization of Euler-Lagrange systems, *Nonlinear Dyn.*, **106** (2021), 445–458. https://doi.org/10.1007/s11071-021-06826-0

33. C. D. Liang, M. F. Ge, Z. W. Liu, L. Wang, J. H. Park, Model-free cluster formation control of NMSVs with bounded inputs: a predefined-time estimator-based approach, *IEEE Trans. Intell. Veh.*, **8** (2022), 1731–1741. https://doi.org/10.1109/TIV.2022.3182992

34. G. Chen, Z. Y. Li, Distributed fixed-time optimization control for multi-agent systems with set constraints, *ACTA Automa. Sin.*, **48** (2022), 2254–2264. https://doi.org/10.16383/j.aas.c190416

35. J. A. Moreno, M. Osorio, Strict Lyapunov functions for the super super-twisting algorithm, *IEEE Trans. Automa. Control*, **57** (2012), 1035–1040. https://doi.org/10.1109/TAC.2012.2186179

36. C. D. Liang, M. F. Ge, Z. W. Liu, G. Ling, F. Liu, Predefined-time formation tracking control of networked marine surface vehicles, *Control Eng. Pract.*, **107** (2021), 104682. https://doi.org/10.1016/j.conengprac.2020.104682

37. C. D. Liang, K. L. Huang, X. S. Zhan, T. Han, Q. Chen, M. F. Ge, Fault-tolerant formation of interlinked marine surface vehicles based on fixed-time distributed optimization, *IEEE Int. Things J.*, in press. https://doi.org/10.1109/JIOT.2025.3631953

38. Q. Chen, M. F. Ge, C. D. Liang, Z. W. Gu, J. Liu, Distributed optimization of networked marine surface vehicles: a fixed-time estimator-based approach, *Ocean Eng.*, **284** (2023), 115275. https://doi.org/10.1016/j.oceaneng.2023.115275

AIMS Press